



Fabrication of CuZn-Based Catalyst via Polyethylene Glycol Surfactant and Supercritical Drying

Journal:	<i>Catalysis Science & Technology</i>
Manuscript ID	CY-ART-05-2020-000961.R1
Article Type:	Paper
Date Submitted by the Author:	31-Aug-2020
Complete List of Authors:	Zhang, Peipei; Department of Applied Chemistry, School of Engineering, University of Toyama Peng, Xiaobo; National Institute for Materials Science, Araki, Yuya; University of Toyama Fang, Yuan; School of Engineering, University of Toyama Zeng, Yan; University of Toyama - Gofuku Campus Kosol, Rungtiwa; University of Toyama Yang, Guohui; School of Engineering, University of Toyama, Applied Chemistry Tsubaki, Noritatsu; School of Engineering, University of Toyama, Department of Applied Chemistry

ARTICLE

Fabrication of CuZn-Based Catalyst via Polyethylene Glycol Surfactant and Supercritical Drying

Received 00th January 20xx,

Peipei Zhang,^a Xiaobo Peng,^{*,b,c} Yuya Araki,^a Yuan Fang,^a Yan Zeng,^a Rungtiwa Kosol,^a Guohui Yang,^{a,d} Noritatsu Tsubaki^{*,a}

Accepted 00th January 20xx

DOI: 10.1039/x0xx00000x

CuZn-based catalysts have been applied in industrial methanol synthesis. However, in alcohol-assisted low-temperature methanol synthesis (LT-MS), preparation of highly efficient CuZn-based catalysts is still a considerable challenge. Here, we report two optimized strategies that use polyethylene glycol (PEG) surfactant and supercritical CO₂ drying in urea co-precipitation method, to synthesize the highly efficient CuZn-based catalysts. The PEG treatment is utilized to enhance porosity and improve surface functional groups of the CuZn-based catalysts, and the supercritical CO₂ drying is employed to increase reduction degree for them. The catalytic results of alcohol-assisted LT-MS reveal that via the two optimized strategies, a CuZn-SC-P5 catalyst exhibits superior catalytic performance. It is significantly different from the CuZn-based catalysts prepared by traditional impregnation method, and also better than the catalysts treated by sole PEG treatment or supercritical CO₂ drying. The present work provides multiple strategies to improve catalytic efficiency, and will be beneficial to explore new approaches in catalyst synthesis.

1. Introduction

Methanol is a key commodity for chemical industries. In last century, the ICI Co. Ltd. developed a widespread method that employed Cu/ZnO/Al₂O₃ catalysts to produce methanol from syngas (CO/H₂).¹⁻⁴ However, high temperature (250 to 300 °C) and high pressure (5.0 to 10.0 MPa) are utilized in this synthesis method. The high temperatures result in thermodynamic limitation for the CO conversion, because methanol synthesis is a strongly exothermic reaction (CO + 2H₂ = CH₃OH, ΔH_{298K} = -90.8 KJ mol⁻¹).^{5,6} The equilibrium conversion of CO is only around 25 % at 300 °C and 50 atm. It is highly desirable to develop low-temperature methanol synthesis (LT-MS). Although several research groups have focused on the LT-MS process (100 to 180 °C), harsh operating conditions prevented them from large-scale industrial applications.⁷⁻⁹

The Brookhaven National Laboratory (BNL) of USA reported a LT-MS in slurry at 100-130 °C and 1.0-5.0 MPa over a strong base catalyst composed of NaH, alcohol and acetate.⁸ However, trace amounts of water (H₂O) or carbon dioxide

(CO₂) in the LT-MS systems can rapidly deactivate the basic catalyst. Another method via methylformate (MF) in liquid phase at 100 °C for LT-MS was first proposed by Christiansen.⁹ The mechanism of this process consists of methanol carbonylation to methyl formate, and hydrogenolysis of the methyl formate to methanol. Wender and co-workers further developed this method via a Cu-Cr/CH₃OK catalyst at a 140-180 °C with 3.8-6.2 MPa. They realized high CO conversion and methanol synthesis rate.^{10,11} However, the deactivation of the alkoxide catalyst has never been solved. To overcome this problem, we have designed alcohol-assisted LT-MS in our previous works, which claimed that the alcohols in the LT-MS remarkably lowered the reaction temperature.¹²⁻¹⁸ But, to date, exploration of highly efficient catalyst is still highly challenging in the alcohol-assisted LT-MS.

CuZn-based catalysts have been widely used in methanol synthesis from syngas (CO/H₂) or CO₂ hydrogenation.¹⁹⁻²² They are usually synthesized using co-precipitation method. In the traditional co-precipitation, routine precipitant (for example, Na₂CO₃, NaOH) is employed to prepare CuO/ZnO precursor. The CuO/ZnO precursor is then dried in air at a temperature above 100 °C. However, the routine co-precipitation process results in a weak porous structure and few surface functional groups for CuZn-based catalyst. The traditional drying process in air at the high temperature further reduces porosity and the number of active sites. The obtained CuZn-based catalysts significantly decrease performance of methanol synthesis. Therefore, it is necessary to alter the traditional co-precipitation method with novel precipitation process and efficient drying technique.

Herein, we present two improvement strategies on the

^a Department of Applied Chemistry, School of Engineering, University of Toyama, 3190 Gofuku, Toyama 930-8555, Japan.

^b National Institute for Materials Science (NIMS), Namiki 1-1, Tsukuba, Ibaraki 305-0044, Japan.

^c Key Laboratory of the Ministry of Education for Advanced Catalysis Materials, Institute of Physical Chemistry, Zhejiang Normal University, Jinhua 321004, China.

^d State Key Laboratory of Coal Conversion, Institute of Coal Chemistry, Chinese Academy of Sciences, Taiyuan 030001, PR China

* Corresponding author: hhpengxiaobo@hotmail.com (Xiaobo Peng), tsubaki@eng.u-toyama.ac.jp (Noritatsu Tsubaki)

Electronic Supplementary Information (ESI) available. See

DOI: 10.1039/x0xx00000x

traditional co-precipitation method for CuZn-based catalysts. Polyethylene glycol (PEG) as a surfactant is utilized in the precipitation process, to enhance porosity and increase surface functional groups for the CuZn-based catalysts.^{23,24} Supercritical CO₂ drying is employed in the drying process to improve the number of active sites for them.^{25,26} We also synthesize the CuZn-based catalysts using traditional precipitation process, drying technique, or impregnation method, to compare the catalysts from the two improvement strategies. The physical and chemical properties of these CuZn-based catalysts are systematically investigated by multiple characterization techniques. Further, we evaluate these CuZn-based catalysts in alcohol-assisted LT-MS, and the catalysts optimized by the two improvement strategies exhibit superior performance at a low temperature of 170 °C.

2. Experimental

2.1 Catalyst preparation

The CuZn-based catalysts were synthesized via a homogeneous urea co-precipitation method. Typically, Cu(NO₃)₂·3H₂O (0.025 mol/L), Zn(NO₃)₂·6H₂O (0.025 mol/L) and deionized water (1480 mL) were added into a beaker, to prepare an aqueous solution. PEG (0.05 mol/L) and urea (0.5 mol/L) were then introduced into the aqueous solution. The mixed solution was stirred and heated on 95 °C for 2 h, to obtain the precipitated precursor. After aging for 24 h at room temperature, the precursor was filtered and washed with deionized water. The solid product was then dried by supercritical phase of CO₂ at a temperature of 35 °C with pressure of 7.5 MPa for 6 h. After the supercritical CO₂ drying, the obtained sample was calcined in air at 350 °C for 1 h, and the resulting catalyst was denoted as CuZn-SC-P3. By using the PEG concentration of 0.08 and 0.13 mol/L, CuZn-SC-P5 and CuZn-SC-P8 were fabricated, respectively, while the other treatment processes were the same as CuZn-SC-P3. CuZn-SC-P0 was also prepared by the same processes, but without the PEG treatment. The series of CuZn-SC-P0, CuZn-SC-P3, CuZn-SC-P5 and CuZn-SC-P8 catalysts were denoted as CuZn-SC-Px (x = 0, 3, 5, 8), as shown in Scheme S1.

To synthesize traditional CuZn-based catalysts for comparison, we also employed conventional drying method to substitute the supercritical drying process. The solid products were dried in air at 120 °C for 12 h, after they were filtered and washed with deionized water. The other treatment processes remained unchanged. Using the traditional drying method, CuZn-P0, CuZn-P5 and CuZn-P8 were obtained by tuning the PEG concentration of 0, 0.08 and 0.13 mol/L, respectively. The series of CuZn-P0, CuZn-P5 and CuZn-P8 catalysts were denoted as CuZn-Px (x = 0, 5, 8). In addition, traditional impregnation method were utilized to synthesize two samples of CuZn-I-SC and CuZn-I. In brief, Cu(NO₃)₂·3H₂O (8.2 g), ZnO powder (5.0 g) and deionized water (5.0 mL) were added into a beaker. The mixture was stirred for 1 h. The deionized water was then removed at 60 °C. The CuZn-I-SC sample was dried by the supercritical phase of CO₂. The CuZn-I sample was dried in

air at 120 °C for 12 h. After the drying process, the two samples were calcined in air at 350 °C for 1 h. To further compare the influence of urea precipitant, the traditional co-precipitation method, using Na₂CO₃ as precipitant, was also employed to synthesize CuZn-Na catalysts. The molar ratio of Cu/Zn was the same as the other CuZn-Based catalysts. In the preparation, the nitrates of Cu and Zn, were firstly dissolved in deionized water. The aqueous solution of Na₂CO₃ (0.05 mol/L) was added dropwise to the nitrate solution, under constant stirring at 75 °C for 1 h. Then, the pH value was kept at 8.0, and the precipitates were aged for 24 h at room temperature. The final samples were obtained by filtration, washing with deionized water, drying at 120 °C, and calcination in air at 350 °C for 1 h.

Before alcohol-assisted LT-MS, all the samples were reduced by a gas mixture of H₂/Ar (5 vol.% H₂) at 220 °C for 10 h with a flow rate of 60 mL/min. The apparatus with a quartz reactor (inner diameter = 15 mm) for the reduced process was shown in Scheme S2. After the reduction, the samples were cooled to room temperature, and then passivated in O₂/N₂ (1 vol.% O₂) atmosphere for 4 h with a flow rate of 30 mL/min.

2.2 Catalyst characterization

The scanning electron microscope (SEM, JEOL JSM-6360LV) was used to analyze surface morphology of the CuZn-based catalysts. The transmission electron microscope (TEM, JEOL JEM-3200Fs) was employed to observe the high-magnification morphology at an acceleration voltage of 200 kV. The X-ray diffraction (XRD) analyses were performed by an X-ray diffractometer (RINT 2400; Rigaku) with Cu K α radiation (40 kV and 20 mA). The mean size of Cu and ZnO was calculated by the Scherrer equation at $2\theta = 43.3^\circ$ and 36.1° , respectively. The elemental composition of the CuZn-based catalysts was determined by X-ray fluorescence (XRF) analysis. The X-ray photoelectron spectroscopy (XPS) analyses were conducted by a Thermo Fisher Scientific ESCALAB 250Xi instrument with an Al K α X-ray radiation source and a chamber for in situ H₂ reduction pretreatment. The nitrogen physisorption was measured by a NOVA2200e analyzer. Before the physisorption analysis, the sample was degassed at 200 °C for 3 h. The specific surface area and average pore size were calculated based on the method of Brunauer-Emmett-Teller (BET) and Barrett-Joyner-Halenda (BJH).

The H₂ temperature programmed reduction (H₂-TPR) was carried out using a BELCAT-B-TT analyzer (BEL Japan Co. Ltd.) with a thermal conductivity detector (TCD). The sample (50 mg) was pretreated at 150 °C by a helium gas (30 mL/min) for 1 h. After the pretreatment, the sample was cooled down to 50 °C. Then, a gas mixture of H₂/Ar (5 vol.% H₂; 30 mL/min) was introduced into the test system. The H₂-TPR profiles were recorded from 50 °C to 900 °C with a rate of 10 °C/min. The specific Cu⁰ surface area and Cu dispersion were determined by N₂O adsorption method. The N₂O adsorption analysis was also conducted on the BELCAT-B-TT analyzer (BEL Japan Co. Ltd.). The sample (50 mg) was also pretreated in a helium gas (30 mL/min) at 150 °C for 1 h, and then reduced by a H₂/Ar gas

(5 vol.% H₂; 30 mL/min) at 220 °C for 2 h. After the sample was cooled down to 60 °C, pulses of N₂O/He gas (10 vol.% N₂O) was introduced into the system, and the total consumption of N₂O was recorded. The CO temperature programmed desorption (CO-TPD) was studied using the same BELCAT-B-TT analyzer. The helium pretreatment and H₂ reduction were also the same as those of the N₂O adsorption analysis. After the temperature was lowered to 50 °C, a gas mixture of CO/Ar (5 vol.% CO; 30 mL/min) was introduced into the system. Then the sample was purged by the helium gas (30 mL/min), and the CO-TPD profile was recorded from 50 °C to 900 °C with a rate of 10 °C/min.

The *in-situ* diffuse reflectance infrared Fourier transform spectroscopy (*in-situ* DRIFT) was carried out on a Thermo Nicolet (NEXUS-470) FTIR spectrometer, equipped with a high-temperature and high-pressure chamber, and a MCT detector. Typically, the sample (10 mg) was loaded into the sample cell, and pretreated by a helium gas (20 mL/min) at 150 °C. The pretreated sample was further reduced using a H₂/Ar gas (5 vol.% H₂; 20 mL/min) at 240 °C for 4 h. After the reduction, the sample was purged by the helium gas, and the background spectra were collected at the different temperatures. Then, CO gas or syngas was introduced into the sample cell, and the *in-situ* DRIFT was recorded at 4 cm⁻¹ resolution with 32 scans.

2.3 Catalyst evaluation

The catalytic tests were performed by a flow-type semi-batch autoclave reactor (inner volume = 85 ml). The sample (3.0 g) and 2-butanol (40 ml) were added into the reactor simultaneously. The 2-butanol was used as solvent, and also acted as catalytic promoter in the system. Then, syngas (H₂/CO/CO₂/Ar = 62.6/29.5/4.9/3.0) with a flow rate of 20 mL/min was introduced into the reactor. After purging the system for 20 min with syngas, the reaction was then carried out at a temperature of 170 °C and pressure of 5.0 MPa for 20 h with continuously stirring. The effluent gas was determined by an online gas chromatograph (Shimadzu, GC-8A) with a thermal conductivity detector (TCD). The liquid products both in the reactor and ice trap were analyzed by an off-line GC (Shimadzu, GC-14B) with a flame ionization detector (FID). The conversions of CO, CO₂ and total carbon, and the product selectivity were calculated as follows:

$$(1) \text{CO Conv. (\%)} = (\text{CO}_{\text{in}}/\text{Ar}_{\text{in}} - \text{CO}_{\text{out}}/\text{Ar}_{\text{out}}) / (\text{CO}_{\text{in}}/\text{Ar}_{\text{in}}) \times 100$$

CO Conv. – CO conversion; CO_{in} – peak area of CO in feed gas; Ar_{in} – peak area of Ar in feed gas; CO_{out} – peak area of CO in effluent gas; Ar_{out} – peak area of Ar in effluent gas.

$$(2) \text{CO}_2 \text{ Conv. (\%)} = (\text{CO}_{2,\text{in}}/\text{Ar}_{\text{in}} - \text{CO}_{2,\text{out}}/\text{Ar}_{\text{out}}) / (\text{CO}_{2,\text{in}}/\text{Ar}_{\text{in}}) \times 100$$

CO₂ Conv. – CO₂ conversion; CO_{2,in} – peak area of CO₂ in feed gas; Ar_{in} – peak area of Ar in feed gas; CO_{2,out} – peak area of CO₂ in effluent gas; Ar_{out} – peak area of Ar in effluent gas.

$$(3) \text{Total Carbon Conv. (\%)} = \text{CO Conv.} \times a/(a + b) + \text{CO}_2 \text{ Conv.} \times b/(a + b)$$

a – CO content in the feed gas; b – CO₂ content in the feed gas.

$$(4) S_i (\%) = A_i f_i / \sum A_j f_j \times 100$$

S_i – selectivity of product i; A_i – peak area for product i; f_i – correction factor from quantitative product i.

$$(5) \text{TOF (h}^{-1}\text{)} = (X_{\text{total}} \times n_{\text{total}}) / (W_{\text{cat.}} \times f_{\text{Cu}} \times d_{\text{Cu}} / M_{\text{Cu}})$$

TOF – turnover frequency; X_{total} – total carbon conversion (%); n_{total} – total carbon number of feed gas per hour (mol/h); W_{cat.} – catalyst weight (g); f_{cu} – weight fraction of Cu in the catalyst (%); d_{cu} – dispersion degree of Cu in the catalyst based on N₂O chemisorption (%); M_{cu} – molar mass of Cu (63.5 g/mol).

$$(6) \text{STY (g kg}^{-1} \text{h}^{-1}\text{)} = (X_{\text{CO}} \times n_{\text{CO}} \times S_{\text{MeOH}} \times M_{\text{MeOH}} / W_{\text{cat.}}) + (X_{\text{CO}_2} \times n_{\text{CO}_2} \times S_{\text{MeOH}} \times M_{\text{MeOH}} / W_{\text{cat.}})$$

STY – space-time yield (g kg⁻¹ h⁻¹); X_{CO} – CO conversion; n_{CO} – CO number of feed gas per hour (mol/h); S_{MeOH} – selectivity of methanol; M_{MeOH} – molar mass of methanol (32.0 g/mol); W_{cat.} – catalyst weight (kg); X_{CO₂} – CO₂ conversion; n_{CO₂} – CO₂ number of feed gas per hour (mol/h).

3. Results and discussion

3.1 CuZn-SC-Px for alcohol-assisted LT-MS

To observe the surface morphology of CuZn-SC-Px catalysts after the calcination, we employed scanning electron microscope (SEM). The results were shown in Fig. 1. The CuZn-SC-P0, synthesized from supercritical CO₂ drying without PEG treatment, formed highly disordered sheet structure (Fig. 1a). The CuZn-SC-P3 and CuZn-SC-P5 displayed more uniform

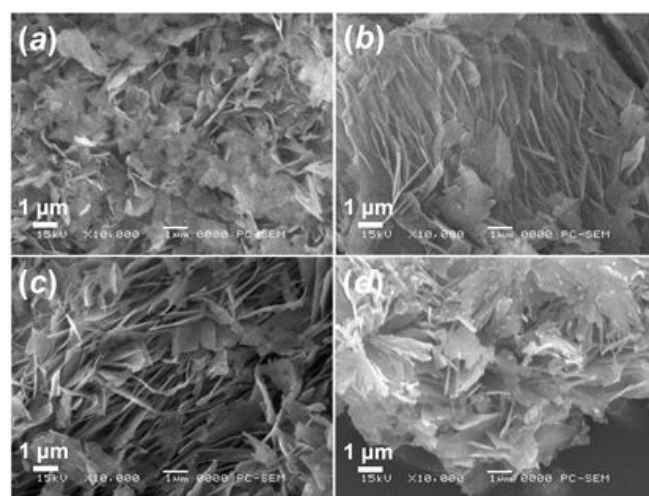


Fig. 1 SEM analyses for the CuZn-SC-Px catalysts after the calcination. (a) CuZn-SC-P0, (b) CuZn-SC-P3, (c) CuZn-SC-P5 and (d) CuZn-SC-P8.

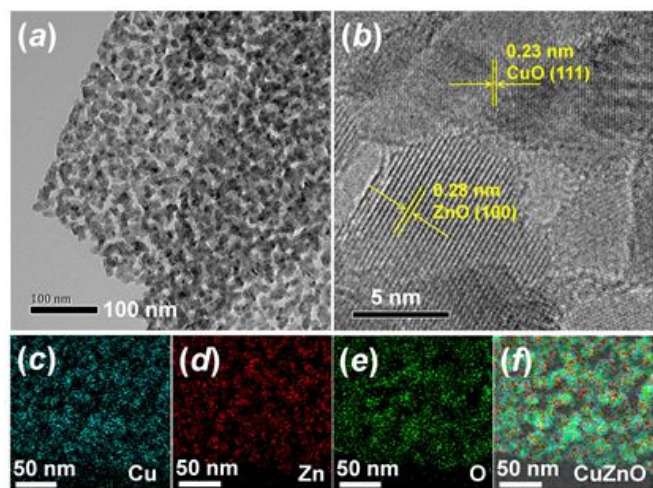


Fig. 2 TEM analyses for the CuZn-SC-P5 catalyst after the calcination. (a) TEM image of the calcined CuZn-SC-P5, (b) high-magnification TEM image of the calcined CuZn-SC-P5; Elemental mapping of the calcined CuZn-SC-P5: (c) Cu, (d) Zn, (e) O (f) Merged.

sheets than the CuZn-SC-P0 (Fig. 1b, c). Moreover, the sheet thicknesses of CuZn-SC-P5 were broader than those of the CuZn-SC-P3. We further counted the thickness of 120 sheets on the CuZn-SC-P5. The average sheet thickness was about 78 nm (Fig. S1). The CuZn-SC-P8 also displayed a sheet structure (Fig. 1d). But the sheet surface of CuZn-SC-P8 generated a large number of bulges, probably due to excessive agglomeration of CuO or ZnO. Compared to the CuZn-SC-P8, the CuZn-SC-P5 possessed a more uniform and smooth sheet surface.

We utilized transmission electron microscopy (TEM) to further observe the sheet structure on the calcined CuZn-SC-P5 (Fig. 2). The TEM results clearly uncovered that a large number of mesopores were formed in the sheet (Fig. 2a), and average size of the metal oxide nanoparticles was about 10 nm (Fig. S2). Moreover, the high-magnification TEM image demonstrated that the nanoparticles of CuO and ZnO were linked to each other (Fig. 2b), and abundant Cu-Zn interfaces were generated in the sheet. The interplanar spacing of 0.23 and 0.28 nm should be attributed to the planes of CuO (111) and ZnO (100), respectively (Fig. 2b).²⁷⁻³⁰ We also applied energy-dispersive X-ray spectroscopy (EDS) to analyze the sheet (Fig. 2c-f). The results revealed that the elements of Cu, Zn, and O were uniform in the whole sheet structure.

The element contents of Cu, Zn and O for all the calcined CuZn-SC-Px catalysts were analyzed by X-ray fluorescence (XRF). As shown in Table 1, the results uncovered that they were almost the same for each CuZn-SC-Px catalyst. To further explore the physical properties, we employed N₂ adsorption-desorption to analyze the calcined CuZn-SC-Px catalysts. Brunauer-Emmett-Teller (BET) area and average pore size were also presented in Table 1. The CuZn-SC-Px catalysts possessed the BET area from 70.7 to 88.5 m²/g, and average pore size from 7.5 to 9.2 nm. The N₂ adsorption-desorption isotherms of CuZn-SC-Px displayed that the CuZn-SC-P3, CuZn-

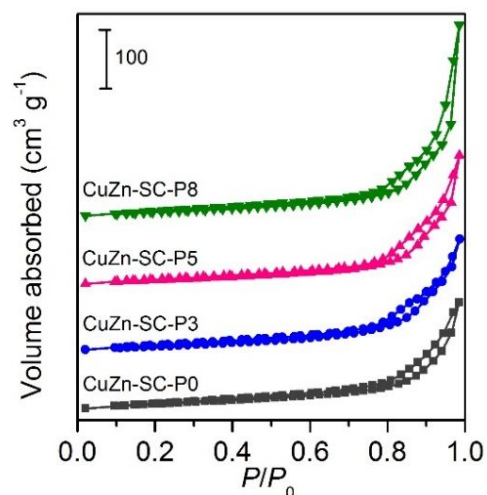


Fig. 3 N₂ adsorption-desorption isotherms for the calcined CuZn-SC-Px.

SC-P5 and CuZn-SC-P8 generated higher BET surface area and volume of adsorbed/desorbed N₂ than the CuZn-SC-P0 (Table 1 and Fig. 3). It suggests that the PEG treatment improved the porous structures on the CuZn-SC-Px. The pore size distribution of the CuZn-SC-Px exhibited that the CuZn-SC-P3 and CuZn-SC-P5 produced larger mesopore size than the CuZn-SC-P0 and CuZn-SC-P8 (Table 1 and Fig. S3). This further indicates that the PEG treatment was beneficial to stabilize the mesoporous structures. But the mesopore size was decreased, when the PEG dosage was too high in the treatment. As a result, the CuZn-SC-P5 obtained a high porosity after the two improvement strategies with the PEG dosage of 5 wt%.

The surface chemical states of CuZn-SC-Px catalysts after the calcination at 350 °C were analyzed using X-ray photoelectron spectroscopy (XPS). The Cu 2p region of CuZn-SC-Px catalysts was indicated in Fig. 4a. The similar Cu 2p peaks imply the same chemical states of Cu species on the CuZn-SC-Px. The Cu 2p 3/2 peaks at 933.4 eV, with the satellite characteristic peaks at around 942.0 eV, clearly demonstrated that the Cu species were divalent cations.^{31,32} In Fig. 4b, the Zn 2p region of Zn-SC-Px was exhibited. The Zn 2p 3/2 peaks at 1021.8 eV was due to ZnO phase, and the shoulder peaks at 1023.7 eV should be attributed to Zn(OH)₂ species.^{33,34} The shoulder peaks of CuZn-SC-P3 and CuZn-SC-P5 were higher than the CuZn-SC-P0 and CuZn-SC-P8, suggesting that the PEG treatment with moderate dosages can result in high distribution of Zn(OH)₂ species. The O 1s region of CuZn-SC-Px was shown in Fig. 4c. The O 1s peaks at 529.4 and 531.4 eV were mainly due to lattice oxygen and surface chemisorbed oxygen, respectively.^{35,36} The increase of the O 1s peaks at 531.4 eV revealed that the high PEG dosage enhanced the content of surface chemisorbed oxygen.

H₂ temperature programmed reduction (H₂-TPR) analyses of the calcined CuZn-SC-Px catalysts were recorded in Fig. 5. They mainly exhibited two peaks for the H₂-TPR profiles. To our knowledge, the peak at low temperature should be ascribed to reduction of highly dispersed Cu species, and the peak at high temperature should be attributed to reduction of

Table 1 Physicochemical properties for the CuZn-based catalysts

Sample	Weight (wt%) ^a			Particle size (nm) ^b		BET area (m ² /g) ^c	Cu ⁰ area (m ² /g) ^d	Cu dispersion (%) ^e	Pore size (nm) ^f
	Cu	Zn	O	Cu	ZnO				
CuZn-SC-P0	37.4	38.6	24.0	8.7	8.7	70.7	22.6	11.7	7.5
CuZn-SC-P3	38.6	38.5	22.9	8.8	9.5	83.7	27.3	12.4	9.0
CuZn-SC-P5	38.6	39.1	22.3	9.6	9.1	88.5	29.8	12.9	9.2
CuZn-SC-P8	37.6	38.7	23.7	9.5	9.9	82.6	25.2	11.8	8.2
CuZn-P0	38.2	35.4	26.4	8.5	8.3	66.5	21.8	11.2	7.7
CuZn-P5	39.0	37.9	23.1	8.9	9.3	82.1	26.2	11.9	8.3
CuZn-P8	38.2	37.7	24.1	13.4	9.6	81.0	24.4	11.3	8.1

(a) Measured by the XRF over the calcined samples. (b) Calculated by the XRD from the reduced samples. The particle sizes of Cu and ZnO were calculated based on the Scherrer equation at $2\theta = 43.3^\circ$ and 36.1° , respectively. (c) Calculated based on the method of BET about the calcined samples. (d) Determined by N₂O chemisorption on the reduced samples. (e) Analysed by N₂O chemisorption from the reduced samples. (f) Evaluated by the BJH method on the calcined samples.

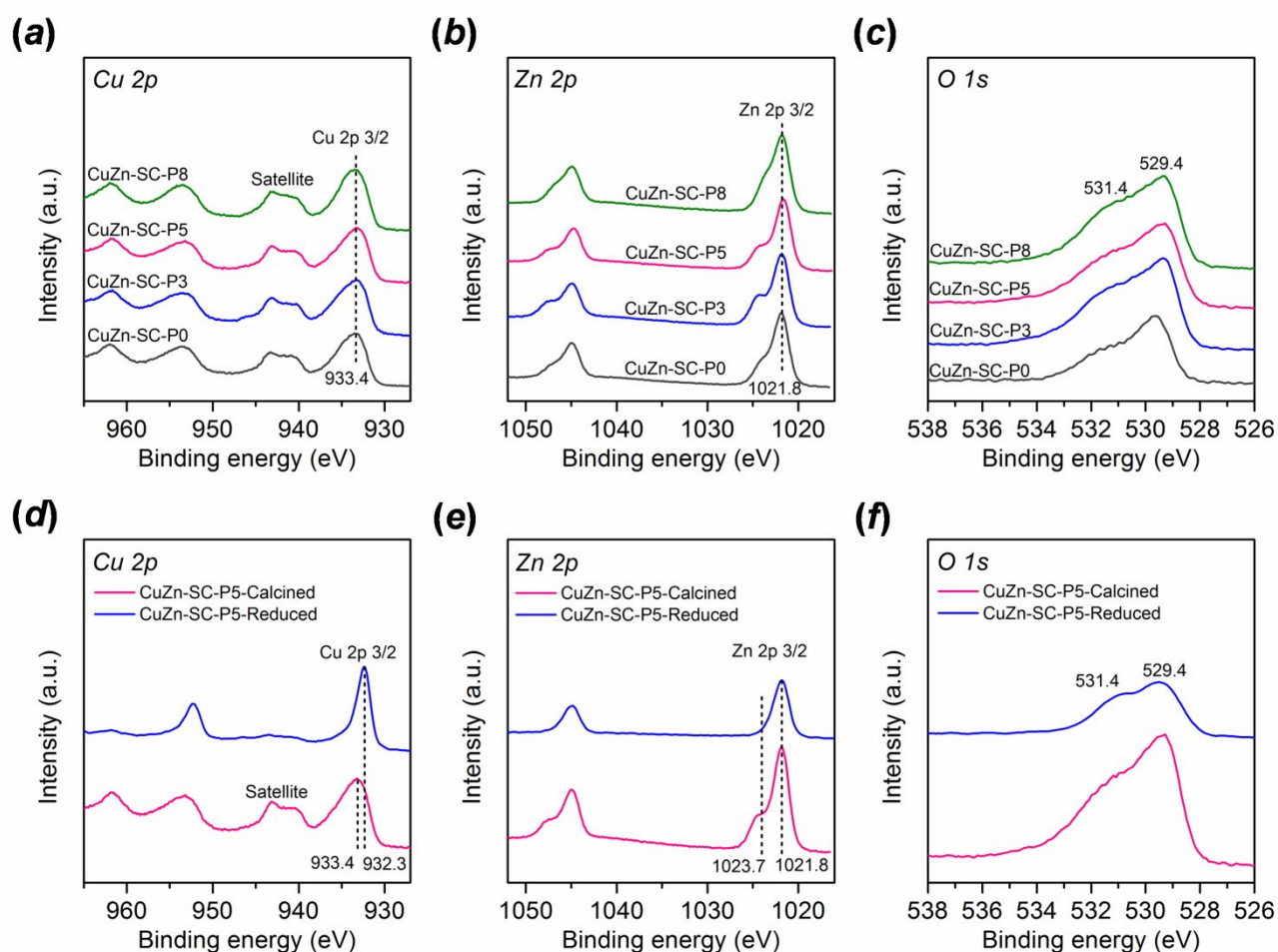


Fig. 4 XPS spectra for the CuZn-SC-Px samples. (a) Cu 2p region for the calcined CuZn-SC-Px, (b) Zn 2p region for the calcined CuZn-SC-Px, (c) O 1s region for the calcined CuZn-SC-Px, (d) Cu 2p region for the CuZn-SC-P5-Calcined and CuZn-SC-P5-Reduced, (e) Zn 2p region for the CuZn-SC-P5-Calcined and CuZn-SC-P5-Reduced, (f) O 1s region for the CuZn-SC-P5-Calcined and CuZn-SC-P5-Reduced.

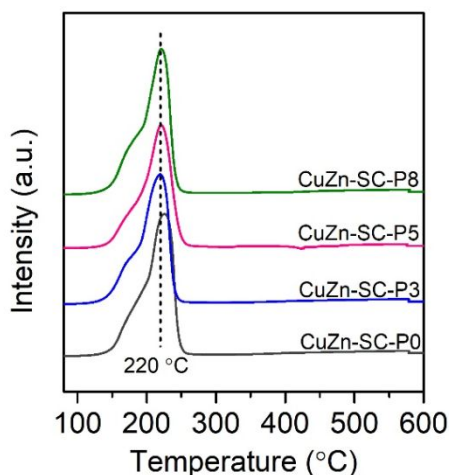


Fig. 5 H₂-TPR profiles for the calcined CuZn-SC-P_x catalysts.

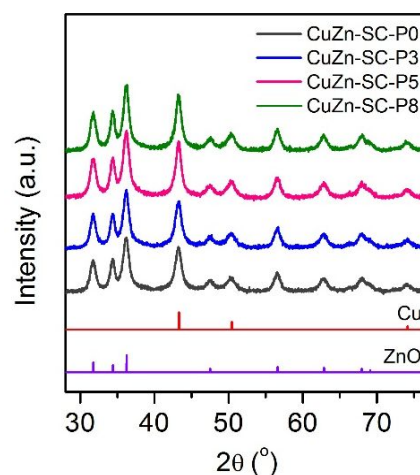


Fig. 6 XRD patterns of the reduced CuZn-SC-P_x catalysts.

bulky CuO particles.³⁷⁻³⁹ As shown in Fig. S4, we also proved this viewpoint via our H₂-TPR analyses of CuZn-based catalysts with different Cu contents. Based on the peak area of Fig. 5, the reduction degrees could reach 70-75 % for these CuZn-SC-P_x catalysts, when the reduction temperature was at 220 °C (Table S1). In addition, the CuZn-SC-P3, CuZn-SC-P5 and CuZn-SC-P8 displayed higher reduction degrees than the CuZn-SC-P0. This observation demonstrated that the PEG treatment enhanced reduction of the Cu species on the CuZn-SC-P_x catalysts.

X-ray diffraction (XRD) patterns of the reduced CuZn-SC-P_x were shown in Fig. 6. The three main peaks at 31.7°, 34.4° and 36.1° should be assigned to the planes of (100), (002) and (101) of ZnO phase, respectively.^{40,41} Another main peak at 43.3° should be due to the (111) plane of Cu phase.^{42,43} We did not observe significant differences for each CuZn-SC-P_x from the XRD analyses. The particle sizes of Cu and ZnO were calculated by the Scherrer equation at $2\theta = 43.3^\circ$ and 36.1° . The calculation results, as indicated in Table 1, revealed that the particle sizes of Cu or ZnO were very close on the CuZn-SC-P_x, although they were prepared by different PEG contents in the co-precipitation process. In contrast, our N₂O chemisorption analysis showed significant differences on Cu⁰ surface area of the reduced CuZn-SC-P_x (Table 1). The CuZn-SC-P3, CuZn-SC-P5 and CuZn-SC-P8 generated higher Cu⁰ surface areas than the CuZn-SC-P0. Moreover, among them the CuZn-SC-P5 possessed the highest Cu⁰ surface area. It indicates that the PEG treatment is also beneficial to improve the Cu⁰ surface area.

To explore the behavior of CO adsorption and activation for the reduced CuZn-SC-P_x catalysts, CO temperature-programmed desorption (CO-TPD) analysis was performed, and the corresponding profiles were displayed in Fig. 7. They mainly exhibited three peaks for CO desorption. One peak below about 250 °C was ascribed to physisorption on the surface of the catalyst.⁴⁴ The other two peaks at about 350 and 400 °C were attributed to the desorption of moderately and strongly adsorbed CO, respectively.⁴⁵ The desorption

temperatures kept almost constant over the reduced CuZn-SC-P_x catalysts, suggesting that the strength of interaction between CO and the Cu surfaces was almost same.⁴⁵ However, the amount of desorbed CO were different among all the samples. As presented in Table S2, the amount of desorbed CO first increased with increasing PEG dosage, and reached a maximum of 0.182 mmol/g over the CuZn-SC-P5. Then it declined with further increasing PEG dosage on the CuZn-SC-P8. This trend was in agreement with that of Cu⁰ surface area, indicating that the higher Cu⁰ surface area was favorable for adsorbing more CO molecules.

We further used *in-situ* XPS analysis to characterize the CuZn-SC-P5 sample. The CuZn-SC-P5, after *in-situ* reduction in the XPS instrument, was analyzed and recorded in Fig. 4d-f (denoted as CuZn-SC-P5-Reduced). It generated lower binding energy of the Cu 2p region than the calcined CuZn-SC-P5 (CuZn-SC-P5-Calcined). The Cu 2p 3/2 peak at 932.3 eV, with the absence of satellite characteristic peaks at around 942 eV (Fig. 4d), implies that the copper species in the CuZn-SC-P5-

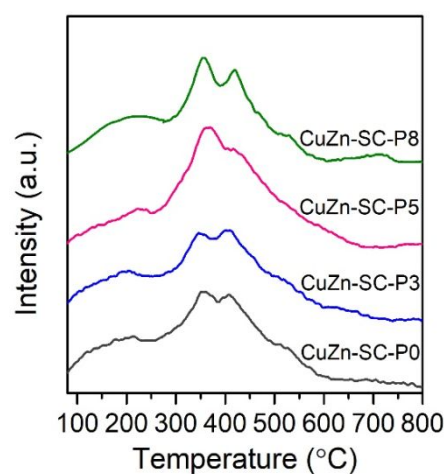


Fig. 7 CO-TPD profiles of the reduced CuZn-SC-P_x catalysts.

Reduced exists as low oxidation state of Cu species (Cu^0 or Cu^{+1}).^{31,32} The Cu (LMM) Auger peaks at 918.6 eV suggests that the Cu^0 was the main phase on surface of the CuZn-SC-P5-Reduced, as depicted in Fig. S5.^{46,47} This is in good agreement with the high reduction degree from H_2 -TPR results. The Zn 2p region uncovered that ZnO was the main species both in the CuZn-SC-P5-Reduced and CuZn-SC-P5-Calcined (Fig. 4e).^{33,34} But the CuZn-SC-P5-Reduced displayed a weak shoulder peak for $\text{Zn}(\text{OH})_2$ species. This implies that the reduction treatment can decrease the concentration of $\text{Zn}(\text{OH})_2$ species. Additionally, the O 1s peaks of CuZn-SC-P5-Reduced revealed a lower intensity of the surface chemisorbed oxygen than that of CuZn-SC-P5-Calcined (Fig. 4f).^{35,36} Therefore, we confirm that the concentration of surface chemisorbed oxygen was lowered via the reduction process. The appropriate reduction temperature should be used to protect surface functional groups and inhibit excessive agglomeration of the Cu nanoparticles.

The catalytic performance of alcohol-assisted LT-MS was evaluated at 170 °C over the CuZn-SC-Px catalysts. Although the product selectivity of CH_3OH , HCOOCH_3 , or 2-butyl formate was very similar on these CuZn-SC-Px catalysts, the conversions of CO and total carbon were significantly different from each other (Table 2). The CuZn-SC-P0 displayed CO conversion of 49.7 % and total carbon conversion of 43.7 %. Compared to the CuZn-SC-P0, the CuZn-SC-P3 and CuZn-SC-P5 produced higher conversions of CO and total carbon. It suggests that the CuZn-SC-Px catalysts with the PEG treatment enhanced the ability of CO conversion. The CuZn-SC-P8 revealed lower conversions of CO and total carbon than the CuZn-SC-P3 and CuZn-SC-P5. This implies that the high dosage of PEG treatment can lead to lowering the activity of alcohol-assisted LT-MS. According to these catalytic results, the CuZn-SC-P5 generated the best performance than the other three CuZn-SC-Px catalysts.

In addition, we also evaluated the stability of CuZn-SC-P5 for alcohol-assisted LT-MS. As shown in Fig. 8, an upward trend during the first 10 h was observed, likely because of the

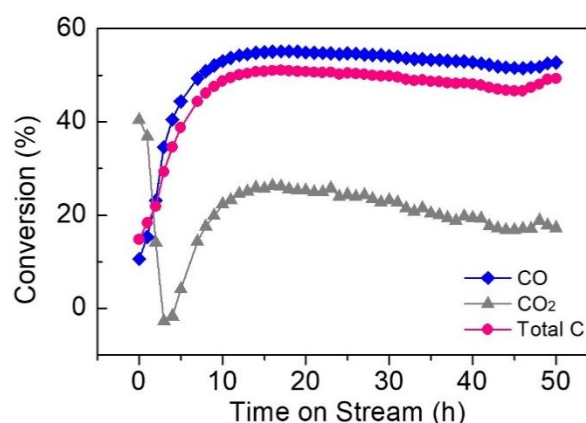


Fig. 8 Stability of the CuZn-SC-P5 catalyst in alcohol-assisted LT-MS. Reaction condition: catalyst weight, 3.0 g; temperature, 170 °C; pressure, 5.0 MPa; solvent, 2-butanol (40 mL); $\text{CO}/\text{CO}_2/\text{H}_2/\text{Ar} = 29.5/4.9/62.6/3.0$; flow rate, 20 mL/min.

dilution influence from dead volume of the initial reactor system. The negative conversion of CO_2 was generated in the initial period, due to extremely low CO_2 concentration in the feed gas and CO_2 formation via water-gas shift reaction. After the test of 50 h, the conversions of CO and total carbon were stabilized at 52.7 and 49.3 %, respectively. These results demonstrated that the CuZn-SC-P5 stably promoted the alcohol-assisted LT-MS reaction at 170 °C.

To further compare the catalytic activity, turnover frequency (TOF) of the total carbon was calculated based on the Cu dispersion, and compared in Table S3. The TOF value increased from 3.29 to 3.31 h^{-1} on the CuZn-SC-Px, and reached a maximum value of 3.40 h^{-1} over the CuZn-SC-P5. But the value lowered to 3.27 h^{-1} on the CuZn-SC-P8 with further increasing the PEG amount. The space-time yield (STY) of methanol for the CuZn-SC-Px was also showed in Table S3. They displayed the same trend as the TOF on the CuZn-SC-Px. The CuZn-SC-P5 generated the maximum methanol STY of 94.7 $\text{g kg}^{-1} \text{h}^{-1}$. To unveil relationship between the copper surface area and the activity of methanol synthesis, we further employed the methanol STY as a function of the exposed Cu^0 surface area of the CuZn-SC-Px (Fig. S6). The results clearly demonstrated that the methanol STY exhibited a good linear relationship with the Cu^0 surface area.

In combination of the characterization results, the CuZn-SC-Px catalysts displayed similar elemental composition and particle size of the copper and zinc. But the XPS results demonstrated that the CuZn-SC-P5 possessed abundant surface Zn-OH hydroxyl groups, which are beneficial to promote the stability of Cu nanoparticles. The N_2 adsorption-desorption and N_2O chemisorption analyses further proved that the CuZn-SC-P5 formed higher porosity and larger Cu^0 surface area than the others. The CO-TPD profile also demonstrated that the CuZn-SC-P5 possessed an excellent behavior of CO adsorption. Therefore, although the CuZn-SC-P3, CuZn-SC-P5 and CuZn-SC-P8 produced similar Cu content and BET surface area, the CuZn-SC-P5 still exhibited the best

Table 2 Catalytic performance of alcohol-assisted LT-MS over the CuZn-SC-Px catalysts

Sample	Conversion (%)			Selectivity (%)		
	CO	CO_2	Total C	CH_3OH	HCOOCH_3	2-Butyl formate
CuZn-SC-P0	49.7	7.2	43.7	96.9	0.2	2.8
CuZn-SC-P3	53.3	2.6	46.1	97.4	0.2	2.4
CuZn-SC-P5	55.8	11.3	49.5	97.4	0.2	2.4
CuZn-SC-P8	50.8	-0.3	43.6	97.7	0.2	2.1

Reaction conditions: catalyst weight, 3.0 g; temperature, 170 °C; pressure, 5.0 MPa; solvent, 2-butanol (40 mL); $\text{CO}/\text{CO}_2/\text{H}_2/\text{Ar} = 29.5/4.9/62.6/3.0$; flow rate, 20 mL/min; time on stream, 20 h.

conversions of CO and total carbon among the CuZn-SC-Px catalysts.

3.2 CuZn-Px for alcohol-assisted LT-MS

We utilized traditional drying method to synthesize the CuZn-Px catalysts. The SEM results exhibited that the calcined CuZn-Px also possessed the sheet structures (Fig. 9). The XRF results demonstrated that they have similar elemental composition (Table 1). In addition, the N₂ adsorption-desorption analyses demonstrated that the CuZn-P5 and CuZn-P8 formed higher BET area than the CuZn-P0. However, compared to the CuZn-SC-P5 from the supercritical CO₂ drying, the CuZn-P5 showed lower BET area and volume of adsorbed/desorbed N₂ (Table 1 and Fig. S7). These phenomena also indicate that the PEG treatment improved the BET area. Moreover, the supercritical CO₂ drying process further promoted the BET area and the porosity.

We further analyzed the chemical states of the calcined CuZn-Px catalysts by XPS (Fig. S8). The Cu 2p region was showed in Fig. S8a. The CuZn-Px catalysts still displayed the same chemical states of the Cu species. The Zn 2p region in Fig. S8b unveiled that the shoulder peaks at 1023.7 eV disappeared on the CuZn-P8. This is consistent with the Zn 2p analyses from the CuZn-SC-Px catalysts. It further implies that the treatment with high PEG dosage inhibited the formation of Zn(OH)₂ species. Although the O 1s peaks revealed that the high dosage of PEG treatment increased the concentration of surface chemisorbed oxygen (Fig. S8c), the CuZn-P8 still displayed larger Cu particle size than the other CuZn-Px after H₂ reduction (Table 1). This indicates that the surface chemisorbed oxygen did not stabilize the Cu particles. By contrast, the surface Zn-OH hydroxyl groups may play a key role on the stability of the Cu particles.

We also employed the H₂-TPR to analyze the calcined CuZn-Px catalysts, as indicated in Fig. S9. The analysis results

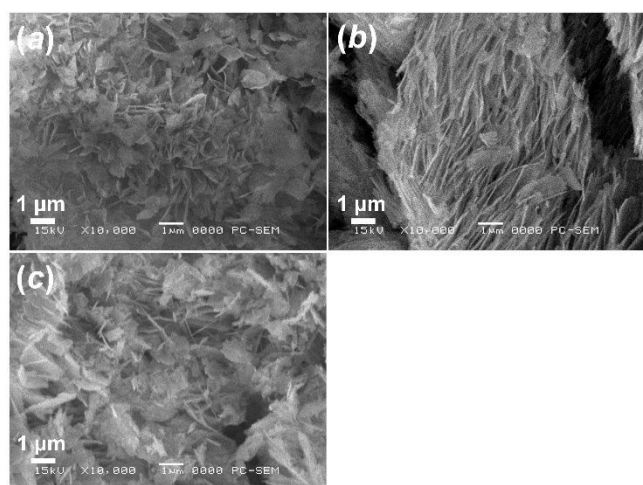


Fig. 9 SEM analyses for the calcined CuZn-Px samples. (a) CuZn-P0, (b) CuZn-P5, and (c) CuZn-P8.

Table 3 Catalytic performance of alcohol-assisted LT-MS over the CuZn-Px catalysts

Sample	Conversion (%)			Selectivity (%)		
	CO	CO ₂	Total C	CH ₃ OH	HCOOCH ₃	2-Butyl formate
CuZn-P0	47.6	5.8	41.7	97.1	0.3	2.6
CuZn-P5	51.4	8.1	45.3	97.8	0.2	2.0
CuZn-P8	44.5	0.7	38.3	96.9	0.3	2.9

Reaction conditions: catalyst weight, 3.0 g; temperature, 170 °C; pressure, 5.0 MPa; solvent, 2-butanol (40 mL); CO/CO₂/H₂/Ar = 29.5/4.9/62.6/3.0; flow rate, 20 mL/min; time on stream, 20 h.

revealed that the reduction degrees were about 58-62 % on the CuZn-Px samples, when the reduction temperature was at 220 °C (Table S1). They were lower than the reduction degrees of 70-75 % on the CuZn-SC-Px catalysts. In addition, we also utilized XRD and N₂O chemisorption to characterize the reduced CuZn-Px catalysts (Table 1 and Fig. S10). The XRD results exhibited that the Cu or ZnO particle sizes of CuZn-P0 and CuZn-P5 were similar with those of the CuZn-SC-Px catalysts. But the CuZn-P8 generated a severe agglomeration for Cu metal, and it formed a larger Cu particle size than the CuZn-SC-P8. The N₂O chemisorption analyses demonstrated that the CuZn-P5 exhibited the best Cu⁰ surface area among the CuZn-Px samples. However, it was still lower than that of the CuZn-SC-P5. These observations clearly showed that the two strategies, PEG treatment and supercritical CO₂ drying, can effectively optimize reduction degree, Cu particle size and Cu⁰ surface area in the preparation processes.

We further tested the catalytic performance of alcohol-assisted LT-MS over the CuZn-Px catalysts. As in Table 3, the CuZn-Px catalysts also displayed similar products selectivities. The methanol selectivity reached about 97 %, and the conversions of CO and total carbon were also different. The CuZn-P0 exhibited the CO conversion of 47.6 % and total carbon conversion of 41.7 %. The CuZn-P8 realized the CO conversion of 44.5 % and total carbon conversion of 38.3 %. Compared to the CuZn-P0 and CuZn-P8, the CuZn-P5 exhibited higher conversions of CO and total carbon. It demonstrated that the appropriate PEG treatment promoted the activity, but the high dosage of PEG treatment decreased the conversions. The XRD and N₂O chemisorption analyses have proved that the high dosage of PEG contents led to large Cu particle size and low Cu⁰ surface area (Table 1). Thus, the CuZn-P5 possessed a better performance than the CuZn-P8.

3.3 Different types of CuZn-based catalysts for alcohol-assisted LT-MS

We applied traditional impregnation method to prepare the CuZn-I catalyst, and further coupled this method with the supercritical CO₂ drying to synthesize the CuZn-I-SC catalyst. The performance of alcohol-assisted LT-MS, over the CuZn-I

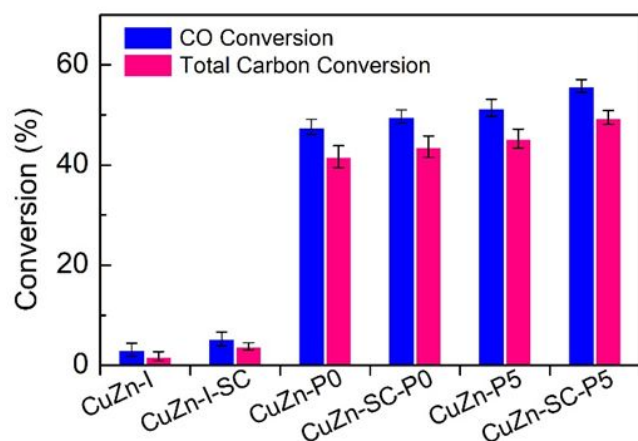


Fig. 10 CO conversion and total carbon conversion over the CuZn-based catalysts from different preparation methods. Reaction conditions: catalyst weight, 3.0 g; temperature, 170 °C; pressure, 5.0 MPa; solvent, 2-butanol (40 mL); CO/CO₂/H₂/Ar = 29.5/4.9/62.6/3.0; flow rate, 20 mL/min; time on stream, 20 h.

and CuZn-I-SC, was exhibited in Fig. 10 and Table S4. The CuZn-I and CuZn-I-SC revealed that conversions of CO and total carbon were about 3-5 %. Although the Cu contents of 35 wt% were the same on the two catalysts, they displayed much lower conversions than the CuZn-Px and the CuZn-SC-Px catalysts. This observation allows us to consider that the impregnation method did not efficiently activate the molecules of CO and H₂ at such low temperature of 170 °C.

In-situ DRIFT spectra of CO adsorption for the CuZn-I-SC and CuZn-SC-P5 were shown in Fig. S11. Before the CO adsorption, the two samples were pretreated by *in-situ* reduction of H₂. Then, the CO adsorption was conducted at room temperature. The results exhibited that the CuZn-SC-P5 generated a very strong CO adsorption. The adsorption peaks at 2103, 2130 and 2168 cm⁻¹ should be ascribed to the CO adsorbed on Cu⁰ and Cu⁺¹ and Cu⁺², respectively.^{48,49} However, the CuZn-I-SC only formed a weak CO adsorption. This further demonstrated that it is difficult to activate the CO molecules on the CuZn-I-SC. In contrast, the CuZn-SC-P5 revealed high intensity for CO adsorption peaks, indicating that it possessed a strong interaction between the CO molecules and Cu surface, and high probability for the CO activation.

In the processes of impregnation method, we employed ZnO powder as the catalyst support. After the impregnation, the Cu particles should be distributed on outer surface of the ZnO powder (Fig. 11a). This resulted in severe agglomeration of Cu to generate large particle size and low probability of the CO activation (Fig. S11 and S12). Moreover, the number of Cu-Zn interface was significantly decreased. It can further accelerate agglomeration and sintering of the Cu species and lower the activity. Consequently, the CuZn-I and CuZn-I-SC displayed low conversion for the alcohol-assisted LT-MS. In contrast, we employed urea co-precipitation method to prepare the CuZn-Px and the CuZn-SC-Px catalysts. The urea was slowly decomposed to produce a uniform basic environment. It can effectively inhibit the severe

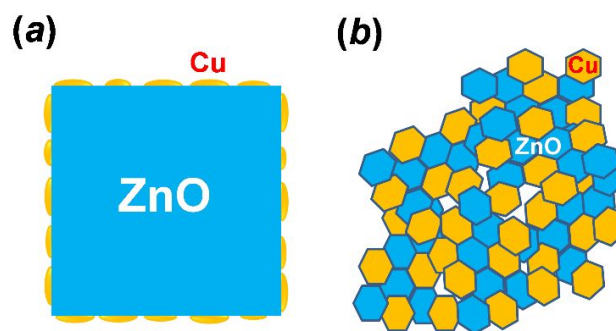


Fig. 11 Schematic illustrations for the CuZn-based catalysts from different preparation methods. (a) Traditional impregnation method and (b) urea co-precipitation method.

agglomeration of Cu, and the uniform and small precipitates can produce a large number of Cu-Zn interface (Fig. 11b). These phenomena have been demonstrated by our characterization analyses of XRD and TEM (Fig. 2, 6 and Table 1). Therefore, the CuZn-Px and CuZn-SC-Px exhibited remarkable improvement on the activity of alcohol-assisted LT-MS.

Compared to the CuZn-I, CuZn-P0 and CuZn-P5 catalysts, the CuZn-I-SC, CuZn-SC-P0, and CuZn-SC-P5 catalysts, prepared from the supercritical CO₂ drying, showed the enhanced performance. The H₂-TPR analyses clearly uncovered that the CuZn-SC-Px possessed higher reduction degrees than the CuZn-Px (Table S1). According to this analysis, the optimized performance of the CuZn-I-SC, CuZn-SC-P0, and CuZn-SC-P5 should be due to the high reduction degrees, caused by the supercritical CO₂ drying. In addition, the CuZn-P5 and CuZn-SC-P5 displayed higher performance than the CuZn-P0 and CuZn-SC-P0. The XPS results have demonstrated that the appropriate dosage of PEG treatment can promote the activity of alcohol-assisted LT-MS. Therefore, we confirm that the PEG treatment was beneficial to enhance the activity. As a result, using the urea co-precipitation method being accompanied by PEG treatment and supercritical CO₂ drying, we obtained the excellent performance of alcohol-assisted LT-MS over the CuZn-SC-P5.

To further compare the influence of urea co-precipitation method, we employed traditional Na₂CO₃ co-precipitation method to prepare CuZn-Na catalyst. The catalytic performance and BET area were showed in Table S5. The CuZn-Na displayed CO conversion of 41.4 % and BET area of 60.2 m²/g. In comparison to the CuZn-Na, the CuZn-P0, synthesized from urea co-precipitation, exhibited higher CO conversion and BET area. Further, the CuZn-SC-P5, synthesized from urea co-precipitation with the PEG treatment and supercritical CO₂ drying, displayed higher CO conversion and BET area than the CuZn-P0. These results demonstrated that the urea co-precipitation method improved the catalytic performance and BET area for the CuZn-based catalysts. Moreover, the PEG treatment and supercritical CO₂ drying can further optimize the CuZn-based catalysts, on the basis of the urea co-precipitation method.

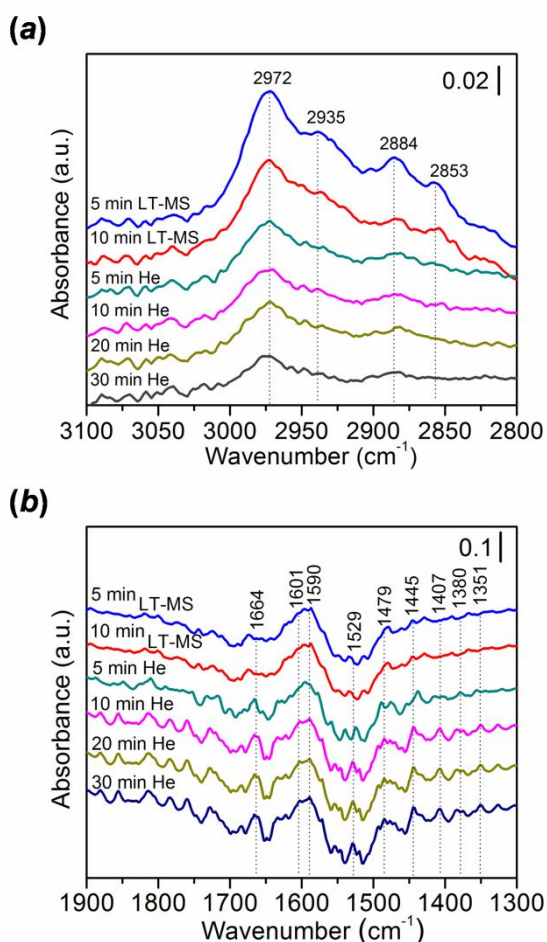


Fig. 12 *In-situ* DRIFT spectra of alcohol-assisted LT-MS over the CuZn-SC-P5. The CuZn-SC-P5 after *in-situ* reduction of H₂ was exposed to syngas with a saturated 2-butanol vapor at 170 °C for 10 min, and then purged in He. Reaction conditions: T = 170 °C, CO/H₂ = 2/1, gas flow rate = 20 mL/min. P = 0.1 MPa. (a) The frequency range from 3100 to 2800 cm⁻¹. (b) The frequency range from 1900 to 1300 cm⁻¹.

To illustrate the mechanism of alcohol-assisted LT-MS, the *in-situ* DRIFT was further performed on the CuZn-SC-P5. The DRIFT results were displayed in Fig. 12. In the range of 3100–2800 cm⁻¹, the IR band at 2972 and 2884 cm⁻¹ should be ascribed to $\nu(\text{CH})$ of 2-butanol and methanol in the adsorption species, respectively. The band at 2935 and 2853 cm⁻¹ was attributed to $\nu(\text{CH})$ of 2-butanol and methanol species in the gas phase, respectively (Fig. 12a).^{12,50} Although the CuZn-SC-P5 was purged in He after 30 min, it still displayed high peak intensity for the 2-butanol adsorption. In the range of 1900–1300 cm⁻¹, we observed an obvious change that the peak intensity increased with the He purge (Fig. 12b). The band at 1664, 1590 and 1380 cm⁻¹ was due to the groups of C=O, OCO and CH₃, respectively.^{12,17} The band at 1500–1400 cm⁻¹ should be attributed to the C-O and C-C stretching vibrations, and the band at 1601 cm⁻¹ was H₂O adsorbed on Cu species.¹² In particular, the band for HCOO–Zn and HCOO–Cu adsorption species was observed at 1529 and 1351 cm⁻¹, respectively.^{12,17} This indicates that the formate was the reaction intermediate. Additionally, we have detected 2-butyl

formate in the reaction products. Therefore, we confirm that the 2-butanol served not only as solvent, but also as catalytic promoter in the system.

4. Conclusions

In conclusion, we have successfully employed PEG treatment and supercritical CO₂ drying to improve traditional coprecipitation method of CuZn-based catalysts for alcohol-assisted low-temperature methanol synthesis (LT-MS). The catalytic reaction results revealed that the CuZn-SC-P5 catalyst, after both improvement strategies, exhibited excellent performance. The conversions of CO and total carbon reached 55.8 and 49.5 %, respectively. Moreover, the CuZn-SC-P5 uncovered much higher conversions than the CuZn-based catalysts prepared by traditional impregnation method, and a better performance than the catalysts treated by sole PEG treatment or sole supercritical CO₂ drying. Our characterization analysis demonstrated that the moderate PEG treatment increased BET area, surface functional groups and Cu⁰ surface area for the CuZn-based catalysts. The supercritical CO₂ drying further optimized these CuZn-based catalysts. This work offers two premium strategies to improve the fabrication processes of CuZn-based catalysts, and also facilitates new catalyst designs in other reaction systems.

Conflicts of interest

There are no conflicts to declare.

Acknowledgements

This work is supported by SATREPS project from JICA and JST of Japanese government and Toyo Tires CO. Ltd. This work is also financially supported by JST-CREST of Japan Science and Technology Agency (Grant Number, 17-141003297). Research fund (2017AA001) from Xinjiang-Tianye Co. Ltd. and Xinjiang government is greatly appreciated.

References

- N. Tsubaki, M. Ito and K. Fujimoto, *J. Catal.*, 2001, **197**, 224–227.
- K. C. Waugh, *Catal. Today*, 1992, **15**, 51–75.
- R. G. Herman, G. W. Simmons and K. Klier, *Stud. Surf. Sci. Catal.*, 1981, **7**, 475–489.
- G. H. Graaf, P. J. J. M. Sijtsema, E. J. Stamhuis and G. E. H. Joosten, *Chem. Eng. Sci.*, 1986, **41**, 2883–2890.
- T. Chang, R. W. Rousseau and P. K. Kilpatrick, *Ind. Eng. Chem. Process Des. Dev.*, 1986, **25**, 477–481.
- N. Tsubaki, J. Zeng, Y. Yoneyama and K. Fujimoto, *Catal. Commun.*, 2001, **2**, 213–217.
- J. Haggin, *Chemical Engineering News*, 1986, **21**, Aug. 4.
- Brookhaven National Laboratory, US patent, 1986, 461479, 4619946, 4623634, 4613623, 1990, 4935395.
- J. A. Christiansen, US Patent, 1919, 1302011.
- Z. Liu, J. W. Tierney, Y. T. Shah and I. Wender, *Fuel Process. Technol.*, 1989, **23**, 149–167.
- V. M. Palekar, J. W. Tierney and I. Wender, 1993, **103**, 105–122.

- 12 R. Yang, Y. Fu, Y. Zhang and N. Tsubaki, *J. Catal.*, 2004, **228**, 23-35.
- 13 J. Zeng, K. Fujimoto and N. Tsubaki, *Energy Fuels*, 2002, **16**, 83-86.
- 14 P. Reubroycharoen, T. Yamagami, T. Vitidsant, Y. Yoneyama, M. Ito and N. Tsubaki, *Energy Fuels*, 2003, **17**, 817-821.
- 15 R. Yang, X. Yu, Y. Zhang, W. Li and N. Tsubaki, *Fuel*, 2008, **87**, 443-450.
- 16 L. Shi, G. Yang, K. Tao, Y. Yoneyama, Y. Tan and N. Tsubaki, *Acc. Chem. Res.*, 2013, **46**, 1838-1847.
- 17 F. Meng, Q. Zhang, G. Yang, R. Yang, Y. Yoneyama and N. Tsubaki, *Chem. Eng. J.*, 2016, **295**, 160-166.
- 18 R. Fan, M. Kyodo, L. Tan, X. Peng, G. Yang, Y. Yoneyama, R. Yang, Q. Zhang and N. Tsubaki, *Fuel Process. Technol.*, 2017, **167**, 69-77.
- 19 T. Fujitani, *J. Japan Pet. Inst.*, 2020, **63**, 43-51.
- 20 S. Kattel, P. J. Ramírez, J. G. Chen, J. A. Rodriguez and Ping Liu, *Science*, 2017, **355**, 1296-1299.
- 21 S. Chen, J. Zhang, P. Wang, X. Wang, F. Song, Y. Bai, M. Zhang, H. Xie, and Y. Tan, *ChemCatChem*, 2019, **11**, 1448-1457.
- 22 A. A. Tountas, X. Peng, A. V. Tavasoli, P. N. Duchesne, T. L. Dingle, Y. Dong, L. Hurtado, A. Mohan, W. Sun, U. Ulmer, L. Wang, T. E. Wood, C. T. Maravelias, M. M. Sain and Geoffrey A. Ozin, *Adv. Sci.* 2019, **6**, 1801903.
- 23 Y. L. Zhang, Y. Yang, J. Zhao, R. Tan, P. Cui and W. Song, *J. Sol-Gel Sci. Technol.*, 2009, **51**, 198-203.
- 24 A. Budiman, M. Ridwan, S. M. Kim, J. W. Choi, C. W. Yoon, J.M. Ha, D.J. Suh and Y.W. Suh, *Appl. Catal. A: Gen.*, 2013, **462-463**, 220-226.
- 25 P. Zhang, Y. Araki, X. Feng, H. Li, Y. Fang, F. Chen, L. Shi, X. Peng, Y. Yoneyama, G. Yang and N. Tsubaki, *Fuel*, 2020, **268**, 117213.
- 26 C. A. García-González, M. C. Camino-Rey, M. Alnaief, C. Zetzl and I. Smirnova, *J. Supercrit. Fluids*, 2012, **66**, 297-306.
- 27 P. C. Rath, J. Patra, D. Saikia, M. Mishra, J. K. Chang and H. M. Kao, *J. Mater. Chem. A*, 2016, **4**, 14222-14233.
- 28 J. Dhakshinamoorthy and B. Pullithadathil, *J. Phys. Chem. C*, 2016, **120**, 4087-4096.
- 29 K. Xu, J. Wu, C. Fu Tan, G. W. Ho, A. Wei and M. Hong, *Nanoscale*, 2017, **9**, 11574-11583.
- 30 Jyoti and G.D. Varma, *J. Alloys Compd.*, 2019, **806**, 1469-1480.
- 31 Y. Wu, E. Garfunkel and T. E. Madey, *J. Vac. Sci. Technol. A*, 1996, **14**, 1662.
- 32 A. Yin, X. Guo, W. Dai and K. Fan, *J. Phys. Chem. C*, 2009, **113**, 11003-11013.
- 33 H.Y. Chen, S.P. Lau, L. Chen, J. Lin, C.H.A. Huan, K.L. Tan and J.S. Pan, *Appl. Sur. Sci.*, 1999, **152**, 193-199.
- 34 G. G. Guillén, M. I. M. Palma, B. Krishnan, D. Avellaneda, G.A. Castillo, T.K.D. Roy and S. Shaji, *Mater. Chem. Phys.*, 2015, **162**, 561-570.
- 35 K. P. Ghoderao, S. N. Jamble and R. B. Kale, *Mater. Res. Express*, 2017, **4**, 105009.
- 36 X. Hou, F. Zhou, B. Yu and W. Liu, *Mater. Lett.*, 2007, **61**, 2551-2555.
- 37 W. Dow, Y. Wang and T. Huang, *J. Catal.*, 1996, **160**, 155-170.
- 38 A. Bansode, B. Tidona, P. R. von Rohr and A. Urakawa, *Catal. Sci. Technol.*, 2013, **3**, 767-778.
- 39 X. Courtois, V. Perrichon, M. Primet and G. Bergeret, *Stud. Surf. Sci. Catal.*, 2000, **130**, 1031-1036.
- 40 R. M. Wang, Y.J. Xing, J. Xu and D.P. Yu, *New J. Phys.*, 2003, **5**, 115.1-115.7.
- 41 J. Wang, Z. Gao, Z. Li, B. Wang, Y. Yan, Q. Liu, T. Mann, M. Zhang and Z. Jiang, *J. Solid State Chem.*, 2011, **184**, 1421-1427.
- 42 H. Zhu, C. Zhang and Y. Yin, *J. Cryst. Growth*, 2004, **270**, 722-728.
- 43 P. K. Khanna, S. Gaikwad, P. V. Adhyapak, N. Singh and R. Marimuthu, *Mater. Lett.*, 2007, **61**, 4711-4714.
- 44 F. Song, Y. Tan, H. Xie, Q. Zhang and Y. Han, *Fuel Process. Technol.*, 2014, **126**, 88-94.
- 45 X. Dong, H. Zhang, G. Lin, Y. Yuan and K. Tsai, *Catal. Letters*, 2003, **85**, 237-246.
- 46 A. Maetaki and K. Kishi, *Surf. Sci.*, 1998, **411**, 35-45.
- 47 J. Batista, A. Pintar, D. Mandrino, M. Jenko and V. Martin, *Appl. Catal. A: Gen.*, 2001, **206**, 113-124.
- 48 A. Dandekar and M. A. Vannice, *J. Catal.*, 1998, **178**, 621-639.
- 49 A. G. Sato, D. P. Volanti, D. M. Meira, S. Damyanova, E. Longo and J. M. C. Bueno, *J. Catal.*, 2013, **307**, 1-17.
- 50 Y. Wang, S. Kattel, W. Gao, K. Li, P. Liu, J.G. Chen and H. Wang, *Nat. Commun.*, 2019, **10**, 1166.

Table of Contents Entry



We employed PEG treatment and supercritical CO₂ drying to improve traditional co-precipitation method of CuZn-based catalysts for alcohol-assisted low-temperature methanol synthesis.